Peer-Reviewed Technical Communication

Merging Multiple-Partial-Depth Data Time Series Using Objective Empirical Orthogonal Function Fitting

Ying-Tsong Lin, *Member, IEEE*, Arthur E. Newhall, *Member, IEEE*, Timothy F. Duda, *Senior Member, IEEE*, Pierre F. J. Lermusiaux, *Member, IEEE*, and Patrick J. Haley

***Abstract*—In this paper, a method for merging partial overlapping time series of ocean profiles into a single time series of profiles using empirical orthogonal function (EOF) decomposition with the objective analysis is presented. The method is used to handle internal waves passing two or more mooring locations from multiple directions, a situation where patterns of variability cannot be accounted for with a simple time lag. Data from one mooring are decomposed into linear combination of EOFs. Objective analysis using data from another mooring and these patterns is then used to build the necessary profile for merging the data, which is a linear combination of the EOFs. This method is applied to temperature data collected at a two vertical moorings in the 2006 New Jersey Shelf Shallow Water Experiment (SW06). Resulting profiles specify conditions for 35 days from sea surface to seafloor at a primary site and allow for reliable acoustic propagation modeling, mode decomposition, and beamforming.**

***Index Terms*—Empirical orthogonal functions (EOFs), Mid-Atlantic Bight, Massachusetts Institute of Technology Multidisciplinary Simulation, Estimation, and Assimilation System (MIT-MSEAS) ocean modeling system, objective function fitting, oceanographic data merging, 2006 Shallow Water Experiment (SW06).**

I. Introduction

In oceanography, it is common for data at individual mooring sites to span only a subsection of the entire water column. A technique is presented here for merging time series of such partial-depth profiles into a time series of profiles intended to describe, as accurately as possible, conditions at a single location. A spatial (depth) overlap in the data sets is a necessary criterion to apply the method. The resulting merged profiles span the entire depth range sampled by the collection of moorings (i.e., the union of the sets). The method can be applied to the situation of internal waves passing over a group of moorings from multiple directions. In the case of waves moving in one direction, it may be possible to merge using a simple time lag of the data. This is not possible in the case of waves passing from many directions, overlapped in time.

The theory and mathematics behind the mooring data merging application presented in this paper are well established. The method uses empirical orthogonal function (EOF) theory [1] to build basis function sets for fluctuations at one location (mooring, in this case). These functions are then used to consistently merge the information in that data set with data from another location. The merging is done using methods of objective function fitting [2], but slightly differs from previous implementations. Data from two or more locations can be merged, but in much of this paper the language is consistent with merging two data sets. Although it is not presented in this paper, the data sources can also be different types; for example, one being *in situ* mooring data and another being model simulation. The technique requires that each profile time series that is to be EOF processed and then merged have an overlap in depth with a primary data set. EOF methods have the beneficial property that the reconstructed fields have the same first- and second-order statistics as the original field, improving the quality of the merged profiles. One advantage of employing EOF analysis is that, if the time series is divided into windows of various lengths, characteristics of the resulting EOFs can provide insight into the nature of water-column profile variation.

EOF theory has been widely applied to analysis of oceanographic profile data. For example, LeBlanc and Middleton [3] first applied EOF analysis to sound-speed data in the Atlantic Ocean. Also, Newhall *et al.* [4] used a spatial EOF interpolation to construct a 3-D sound-speed field for acoustic ray tracing modeling. In addition to these applications to sound-speed data, Duda and Rehmann [5] applied an EOF filter on their acoustic Doppler current profiler (ADCP) data for the purpose of reducing noise without losing vertical resolution. Multivariate model-predicted time-dependent 3-D EOFs have also been used to describe dominant uncertainties for data assimilation [6]. In these studies, the entire data set under consideration is used to build EOFs, which are then used to reconstruct a field. In contrast, in the present work, only a portion of the total data

Manuscript received April 06, 2009; revised December 22, 2009 and May 12, 2010; accepted May 17, 2010. Date of publication October 18, 2010; date of current version November 30, 2010. This work was supported by the U.S. Office of Naval Research (ONR) under Grants N00014-04-1-0146 and N00014-05-1-0482, the ONR Postdoctoral Fellowship Award under Grant N00014-08-1-0204, and by E. Livingston and T. Pawluskiewicz. The work of P. F. J. Lermusiaux and P. J. Haley was supported by the ONR under Grants N00014-07-1-1061, N00014-07-1-0501, and N00014-08-1-1097 to the Massachusetts Institute of Technology.

Associate Editor: R. Chapman.

Y.-T. Lin, A. E. Newhall, and T. F. Duda are with the Applied Ocean Physics and Engineering Department, Woods Hole Oceanographic Institution, Woods Hole, MA 02543 USA (e-mail: ytlin@whoi.edu; anewhall@whoi.edu; tduda@whoi.edu).

P. F. J. Lermusiaux and P. J. Haley are with the Massachusetts Institute of Technology, Cambridge, MA 02139 USA (e-mail: pierrel@mit.edu; phaley@mit.edu).

Color versions of one or more of the figures in this paper are available online at http://ieeexplore.ieee.org.

Digital Object Identifier 10.1109/JOE.2010.2052875

set is used to build EOFs, and other data are used to construct fields using those EOFs as basis functions.

Objective analysis [1], [7] and objective function fitting [2] are commonly used in the natural sciences. These methods are often used to find patterns of variation in sparse and/or noisy data sets, sometime using EOFs as basis functions [2]. Maps of fields that result from the procedure fill space, so the term optimal interpolation has also been used for this. In this paper, the objective analysis is used in slightly different way. Interpolation is not the goal. Rather, the merging procedure first uses data from one location to build basis functions (i.e., EOFs), then uses independent new data from another location to find the linear combination of basis functions that forms a profile consistent with the new data. The merging procedure is not a large departure from traditional usage. However, there are some new aspects that form the major results reported here. First, the statistics and EOFs are allowed to be time dependent, as has been done in data assimilation context where the governing partial differential equations are used to evolve these EOFs [6], [8]–[10]. Here the EOFs are evolved by time-variable windowing, and a large part of the effort involves the analysis of changing EOF sets, and how to determine the time scales of data windowing used in the analysis.

Acoustic propagation prediction is one discipline that requires full-depth profiles, namely, of sound speed. After an explanation of the method, its application is illustrated by generating temperature profiles using data collected in summer 2006 during a large multidisciplinary project, the 2006 New Jersey Shelf Shallow Water Experiment (SW06) [11]. The merged temperature profiles are then joined with other salinity information to form full-depth sound-speed profiles.

This paper is organized as follows. In Section II, the merging method is described in detail and compared with a related method [2]. Section III shows SW06 temperature data merging and an analysis of error. Section IV briefly examines how the merged temperature profiles, converted to sound speed, improve acoustic navigation system performance. Sections V and VI have discussions, conclusions, and suggestions for future work.

II. Method

The merging method is described here. A basic requirement for the method to be appropriate is that water-column variability is caused by passing features whose signature can be represented by empirical fundamental functions derived from the first- and second-order statistics. In ocean acoustic studies, these features are often internal waves, with time scales of a few minutes to a few hours. For data source moorings only a few hundred meters apart, the statistics should be identical (stationarity holds). Hence, the empirical fundamental functions derived from one mooring data set are applicable to representing the water-column variability at the other mooring location. Another important underlying assumption is that the local fundamental functions vary with a slow time scale of order tens of minutes, and so they can be efficiently and sufficiently estimated within a finite time window.

A. Description

In this merging method, samples from a primary data set, which covers the majority of the water column and remains intact, are augmented using the secondary data set that covers an additional portion of the water column. The remaining description of this method assumes a single secondary data set, but more than one secondary data set can be used. In principle, the procedure can be extended to multivariate fields and higher spatial dimensions.

The first step of this merging method is to determine the time-dependent first- and second-order statistics of the secondary data series $y_{\rm sec}(\mathbf{z},t)$, where the column vector $\mathbf{z}$ consists of the sensor depths and the total number of the secondary data sensors is M. This computation can be done by continuously moving a time window over the entire data period. This moving window processing yields a series of data averages (the first-order statistics) $\bar{y}_{\rm sec}(\mathbf{z},t)$ and a series of data covariance matrices (the second-order statistics) $\mathbf{\Gamma}^{\rm sec}_{M\times M}(t)$. To determine the needed parameterization of the secondary-data variability, EOF analysis is performed within time windows centered at each analysis time t. At each step of the windowing process, a set of eigenvectors is derived from the corresponding covariance matrix by solving the eigenvalue problem

$$\mathbf{\Gamma}^{\rm sec}_{M\times M}\mathbf{H}_{M\times M}=\mathbf{H}_{M\times M}\mathbf{\Lambda}_{M\times M} \tag{1}$$

where the time variable t is dropped for the purpose of notation simplification and will be done in the following matrix equations. In the equation, the matrix $\mathbf{H}$ contains the eigenvectors $\mathbf{h}_k$ in columns labeled $k=1$ to M. These eigenvectors are the empirical fundamental functions describing variability during the time window, centered at time t. These are also known as the EOFs [1]. The diagonal matrix $\mathbf{\Lambda}$ contains the eigenvalues, and each eigenvalue is the data variance that the corresponding EOF captures.

Before detailing the remaining procedures of augmenting the primary data, we will define a useful depth notation. On the secondary data mooring, the bottom N sensors are overlapping with the primary data mooring, and we use $\mathbf{z}_2$ to denote the overlapped sensor depths. On the other hand, we use $\mathbf{z}_1$ to indicate other sensor depths where the primary data will be augmented. With this depth notation, we can partition the covariance matrix of secondary data into different depth ranges, i.e.,

$$\mathbf{\Gamma}^{\rm sec}=\begin{bmatrix}\mathbf{\Gamma}^{\rm sec}_{11} & \mathbf{\Gamma}^{\rm sec}_{12}\\ \mathbf{\Gamma}^{\rm sec}_{21} & \mathbf{\Gamma}^{\rm sec}_{22}\end{bmatrix} \tag{2}$$

where the element $\mathbf{\Gamma}^{\rm sec}_{ij}$ $(i,j=1 \text{ or } 2)$ is the autocovariance or cross covariance between the secondary data in the depth ranges $\mathbf{z}_i$ and $\mathbf{z}_j$, and $\mathbf{\Gamma}^{\rm sec}_{12}=\mathbf{\Gamma}^{\rm sec}_{21}$. Simple matrix manipulation also shows that

$$\mathbf{\Gamma}^{\rm sec}_{ij}=\mathbf{H}_i\mathbf{\Lambda}\mathbf{H}_j^T \tag{3}$$

where the subscribed $\mathbf{H}$ indicates the portion of the EOFs in the corresponding depth range ($\mathbf{z}_1$ or $\mathbf{z}_2$).

With the secondary-data EOFs, $\mathbf{h}_k$ ($k=1$ to M), the extension profile (in the depth range $\mathbf{z}_1$) can be determined by adding

the mean profile of secondary data and a linear combination of the EOFs

$$y_{\rm pri}(\mathbf{z}_1,t)=\bar{y}_{\rm sec}(\mathbf{z}_1,t)+\sum_{k=1}^{M}h_k(\mathbf{z}_1,t)\alpha_k(t). \tag{4}$$

The coefficients $\alpha_k(t)$ will be determined, in a least square sense, from the data in the overlapped depths of the two data moorings $\mathbf{z}_2$. Note that the whole EOF set is used. The determination of α_k should ideally take into account the fact that the data variance each EOF captures varies with the EOF number; in other words, the extended primary data should have the same EOF spectrum as the secondary data. Clearly, a requirement for this step is that the statistics (up to second order) of both data sets are identical. If this is not true, then using this method to extend the primary data profiles into the depth domain of secondary data is less justifiable.

To determine $\alpha_k(t)$, we first linearly interpolate data from primary sensors that overlap with the secondary-data depth range to the overlapped secondary-data sensor depths and name them $\hat{y}_{\rm pri}(\mathbf{z}_2,t)$, where the size of the vector $\mathbf{z}_2$ is N, as defined previously. Indeed, this interpolation is a source of error, and the error [$\mathbf{e}=\hat{y}_{\rm pri}(\mathbf{z}_2,t)-y_{\rm pri}(\mathbf{z}_2,t)$, where $y_{\rm pri}$ is the actual (unmeasured) primary data value at depths $\mathbf{z}_2$] will be taken into account when determining α_k. By changing the depths of concern in (4) and inserting $\hat{y}_{\rm pri}(\mathbf{z}_2,t)$, we then form a least square fitting problem to solve for α_k

$$\Delta y(\mathbf{z}_2,t)=\sum_{k=1}^{M}h_k(\mathbf{z}_2,t)\,\alpha_k(t) \tag{5}$$

where $\Delta y(\mathbf{z}_2,t)=\hat{y}_{\rm pri}(\mathbf{z}_2,t)-\bar{y}_{\rm sec}(\mathbf{z}_2,t)$. This is an objective function fitting process [2]. The number N is smaller than M (the number of the overlapped sensors is smaller than the total sensor number), and the system is thus underdetermined. Note that only a portion of the EOFs in depths $\mathbf{z}_2$ is used in this objective function fitting procedure.

To solve (5) for α_k while accounting for the EOF energy/variance spectrum and for the interpolation error/uncertainties $\mathbf{e}$, we can form an objective function J to be minimized

$$J=\boldsymbol{\alpha}^T\boldsymbol{\Lambda}^{-1}\boldsymbol{\alpha}+\mathbf{e}^T\boldsymbol{\Sigma}^{-1}\mathbf{e} \tag{6}$$

where $\boldsymbol{\alpha}$ is the column vector consisting of $\alpha_k(t)$, $\boldsymbol{\Lambda}$ is the EOF eigenvalue matrix (note again that each eigenvalue is the data variance that the corresponding EOF captures), and $\boldsymbol{\Sigma}$ is the covariance matrix of the interpolation error $\mathbf{e}$. The first term in the function J is the weighted mean square of the EOF coefficients. This is included to minimize the energy of the fitted solution. The second term is the mean square error between the fitted field and the true field. The matrix $\boldsymbol{\Sigma}$ is essentially unknown, but it can be estimated from the primary data difference within the overlapped depth range; the simplest probability model one can use is the zero-mean uniform probability function with a width given by the data difference. The solution that minimizes the objective function is the well-known tapered and weighted least square solution [12] given by

$$\hat{\boldsymbol{\alpha}}=\left(\boldsymbol{\Lambda}^{-1}+\mathbf{H}_2^T\boldsymbol{\Sigma}^{-1}\mathbf{H}_2\right)^{-1}\mathbf{H}_2^T\boldsymbol{\Sigma}^{-1}\Delta\mathbf{y} \tag{7}$$

where $\mathbf{H}_2$ is the portion of the EOFs in depths $\mathbf{z}_2$, and $\Delta\mathbf{y}$ is the column vector of $\Delta y(\mathbf{z}_2,t)$.

There is another way to write this estimator expression relating to the best estimate and the data points ($\Delta\mathbf{y}$). Using the matrix inverse lemma, one can write

$$\hat{\boldsymbol{\alpha}}=\boldsymbol{\Lambda}\mathbf{H}_2^T\left(\boldsymbol{\Sigma}+\mathbf{H}_2\boldsymbol{\Lambda}\mathbf{H}_2^T\right)^{-1}\Delta\mathbf{y} \tag{8}$$

so that the final extension profile can be expressed as

$$y_{\rm pri}(\mathbf{z}_1,t)=\bar{y}_{\rm sec}(\mathbf{z}_1,t)+\boldsymbol{\Gamma}_{12}^{\rm sec}\left(\boldsymbol{\Sigma}+\boldsymbol{\Gamma}_{22}^{\rm sec}\right)^{-1}\Delta y(\mathbf{z}_2,t) \tag{9}$$

where $\boldsymbol{\Gamma}_{12}^{\rm sec}=\mathbf{H}_1\boldsymbol{\Lambda}\mathbf{H}_2^T$ and $\boldsymbol{\Gamma}_{22}^{\rm sec}=\mathbf{H}_2\boldsymbol{\Lambda}\mathbf{H}_2^T$ are used. This is the Gauss–Markov estimator for objective mapping [12], or objective interpolation. Thus, the method we have chosen, although explained here in terms of EOFs, for reasons to be explained later, is precisely this established method.

In general, there is no strict regulation for selecting the weights used in the objective function (6) for the least squares estimate of the EOF coefficients. However, choosing the two special weights $\boldsymbol{\Lambda}$ and $\boldsymbol{\Sigma}$ recovers a rewritten version of the Gauss–Markov estimator (9) as the achieved solution (7). While it is true that one can directly use (9) to obtain the extension profile of primary data set and skip the EOF decomposition procedure, it is shown later in our data-analysis example that there are advantages to employing EOFs to gain insight into the nature of water-column profile variations. This is also done in data assimilation context [6], [8].

In Section III, the method is applied to the SW06 data. The resulting full-depth profiles are shown. In addition, the performance of the method is tested by rebuilding secondary-data profiles directly from its partial data. In the remainder of this section, we will compare our method with an objective function fitting method examined by Davis [2].

B. Comparison With an Objective Function Fitting Method

Davis [2] analyzed an objective function fitting method for spatial data smoothing or objective mapping. There is a close relationship between the pioneered procedure by Davis and the merging procedure proposed here. The difference is that our method uses a tapered and weighted EOF approach, and Davis' method uses a selected-EOF approach.

In the method outlined here, the augmentation of the primary data set is formed using all EOFs. However, if only a subset of the EOFs are used, of quantity $K<N$, those with the highest eigenvalue, typically, where N is the number of secondary sensors within the overlap, the least square problem is overdetermined. This is in contrast to the underdetermined situation in the originally posed problem (5). Removing the least square term of EOF coefficients from the prior objective function forms a new one, i.e.,

$$J_{\mathbf{e}}=\mathbf{e}^T\boldsymbol{\Sigma}^{-1}\mathbf{e} \tag{10}$$

and yields a new least square solution for α_k [12]

$$\hat{\boldsymbol{\alpha}}_K=\left(\mathbf{H}_{2,K}^T\boldsymbol{\Sigma}^{-1}\mathbf{H}_{2,K}^T\right)^{-1}\mathbf{H}_{2,K}^T\boldsymbol{\Sigma}^{-1}\boldsymbol{\Delta}\mathbf{y} \tag{11}$$

where $\hat{\boldsymbol{\alpha}}_K$ consists of the K highest order EOF coefficients, and the matrix $\mathbf{H}_{2,K}$ contains the K highest order EOFs at depths

TABLE I
ENVIRONMENTAL SENSORS ON THE ASIS SPAR BUOY AND TETHER

Sensor type	Nominal sensor depth (m)	Sampling interval (seconds)
Spar Buoy, Temperature	2	2
Spar Buoy, Temperature	4	60
Spar Buoy, Temperature	6	2
Spar Buoy, Temperature/Pressure	7	4
Tether, Temperature	9	210
Tether, Temperature	12	210
Tether, Temperature/Pressure	15	4

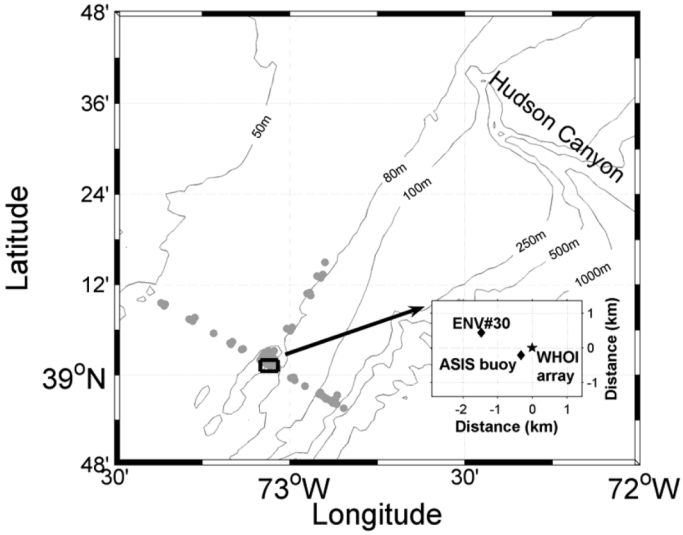

Fig. 1. Study area of SW06. The depth of each isobath line is labeled. A total of 62 moorings, denoted by gray dots, were deployed in a "T" geometry to create an along-shelf path and an across-shelf path. The inner panel is a magnification of the indicated black box and shows the detailed positions of the three moorings whose data are used for full water-column profile estimation at the WHOI array location.

$\mathbf{z}_2$. This is also the solution to the objective function fitting problem posed by Davis [2]. Note that Davis' solution [2, eq. (13b)] is written in summation form, but is identical to (11).

Thus, we can see one connection between the presented solution (7) or (8), which is tapered and weighted, and that of Davis (11). In our approach, the augmentation of the primary data set uses the entire EOF set and weights the coefficients according to the EOF spectrum. Davis' work implements a lowpass filter and effectively uses only the highest order fundamental functions to model the smoothed field data, with unity weighting of each. Because the ocean usually has a red spectrum, the first few dominant fundamental functions usually capture most of the signal information. Thus, for the objective mapping/smoothing purpose, the selected-EOF approach is adequate. In our data merging problem, we wish to retain abrupt transitions at the thermocline and cannot tolerate smoothing. Hence, we should keep the whole EOF set and the statistics intact, with the statistics (the covariance matrix and the associated EOFs) containing the desired information. Finally, we note that our approach can be simply seen as the tapered generalization of that of Davis [2], and the diagonal elements of the tapering matrix Λ set how much weight each EOF has in the final answer.

III. SW06 TEMPERATURE MOORING DATA MERGING

This section provides information about the data sources used in an example application of the method, then the results, including an error analysis. The data to be merged are from temperature sensors attached to a hydrophone vertical line array (VLA) prepared and deployed by the Woods Hole Oceanographic Institution (WHOI, Woods Hole, MA) during SW06 [11], and from an air–sea interaction spar (ASIS) buoy [13] and its tether prepared by the University of Miami (Miami, FL). The WHOI VLA temperature data are primary, and the ASIS temperature data are secondary. The positions of these two moorings are shown in the inner panel of Fig. 1.

A. SW06 Temperature Mooring Data Sources

The primary mooring is the WHOI VLA. Nine temperature sensors and one temperature/pressure sensor attached to this array are used as primary data. These were retrieved at the end of a 43-day SW06 experiment. Temperature was measured at 30-s intervals at the following depths: 13, 15, 19, 22, 26, 34, 41, 56, 71, and 78 m. Pressure was also measured at the uppermost sensor. The top panel of Fig. 2 shows the WHOI VLA temperature data. One can see that the mixed-layer structure was not completely measured, especially when the mixed-layer thickness was less than 13 m.

The secondary mooring is the ASIS. This spar buoy and its tether were floating at the surface to measure air–water interaction. The position was ~385 m southwest of the WHOI VLA. Five temperature sensors and two temperature/pressure sensors were attached to the mooring in the upper 15 m of the water column. See Table I for the nominal sensor depths, and the second panel of Fig. 2 for the temperature data. These data overlapped the primary WHOI VLA data by two sensors $(N = 2)$

For the best possible depth profile reconstruction, it is important to consider the water depth and the sensor array tilt because both influence the sensor depths. The seafloor depth was estimated using the shipboard echo sounder at the time of array deployment. The tidal records registered on an SW06 wave gauge are used to correct the echo sounder data. The resultant value is nominally 78.8 m. A time series of tide-modulated water depths

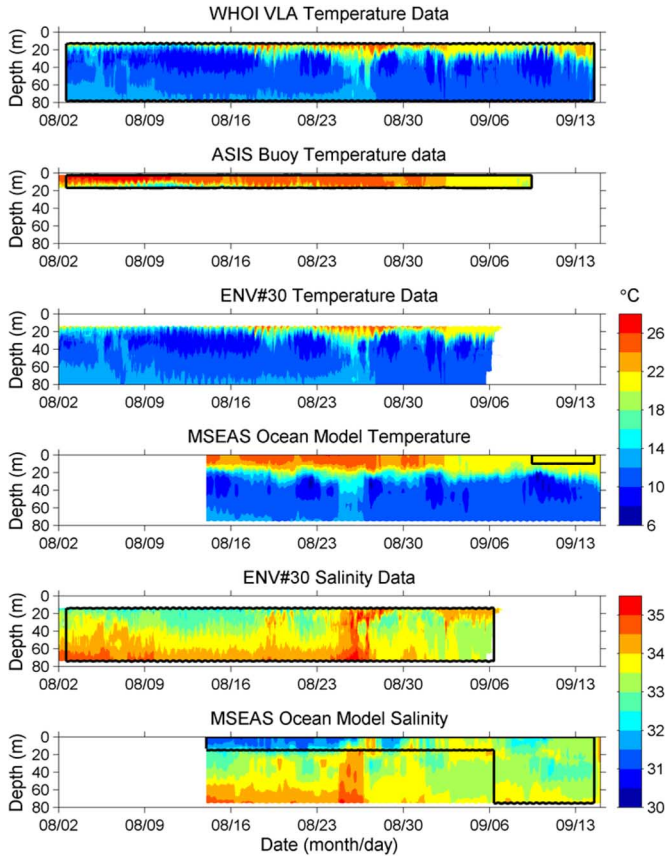

Fig. 2. WHOI VLA temperature data, ASIS temperature data, ENV#30 temperature and salinity data and MSEAS ocean model simulations. The black boxes indicate the data sources for the water temperatures and salinities; WHOI VLA, ASIS buoy, and MSEAS ocean model are the temperature data sources, and ENV#30 and MSEAS ocean model are the salinity data sources.

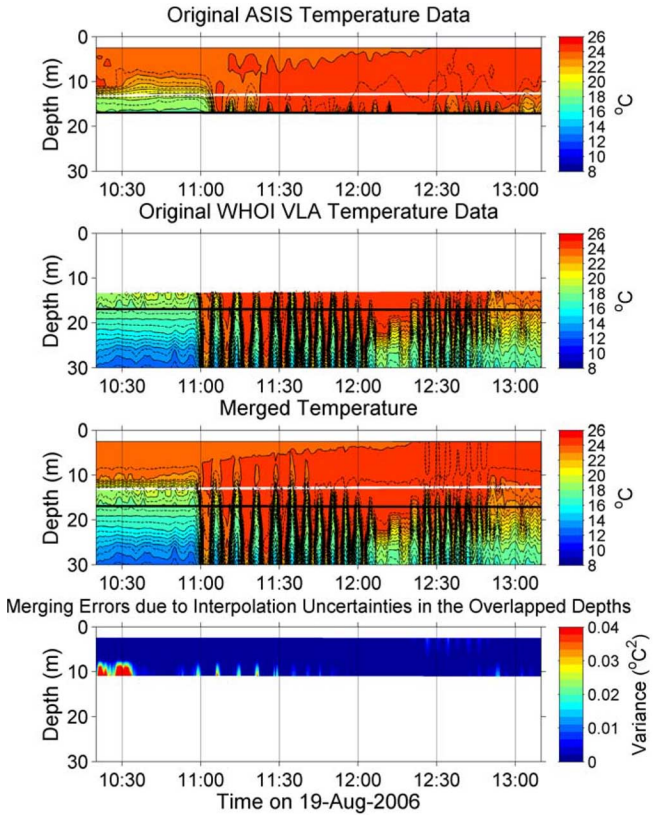

Fig. 3. Contour plots of the original ASIS buoy, WHOI VLA temperature data, and the merged profiles during the largest SW06 internal wave event. The EOF merging technique presented in this paper preserves the mixed layer structure measured by the ASIS buoy in the merged profiles as can be seen in this figure. Contour level increment is 1° in colors and 0.5° in lines. The bottom panel shows the estimated error variance due to the interpolation error/uncertainties in the overlapped depth range.

during the array operational period is calculated considering resolved tidal constituents of frequency at eight cycles per day or less. The semidiurnal M2 tide dominates, with amplitude of about 0.5 m (1 m peak to peak). A long-baseline navigation study for the WHOI VLA [14] shows that the average tilt angle of the array is only $\sim 1.5°$, so the effect of mooring tilt on the VLA sensor depths is minimal and it is thus neglected in this data merging example. The tilt may be more significant for the ASIS spar buoy and its tether. To take the buoy tilt into account, the lowpass filtered pressure records (cutoff frequency eight cycles per day), from two pressure sensors at nominal depths of 7 and 15 m, are used to adjust the sensor depths.

B. Data Merging and Results

The merging method presented in Section II is used to merge the WHOI VLA (primary) and ASIS (secondary) temperature data. A one-hour central boxcar window moving through the entire data time series is used to determine the time series of statistics (means and covariances) and of EOFs. The reason for choosing a one-hour-long window is that it is longer in time scale than the nonlinear internal waves, and longer in time scale than the intermooring wave transit times, but short enough in scale to expect reasonable stationarity.

Data merging results during the largest measured nonlinear internal wave event of SW06 (on August 19th) are specifically selected to be shown here. The temperature data from the VLA and ASIS (top two panels of Fig. 3) indicate significant thermocline displacements of order 25 m in this internal wave packet. The merged temperature profiles are shown in the third panel of Fig. 3. The results appear usable, but this is not sufficient to judge the accuracy. A performance examination (error analysis) of the merging method over the entire experimental period is presented in Section III-C, with additional information provided for this time period.

As explained, the time-dependent statistics of the ASIS data are first calculated, and the resulting average profiles and EOF sets are then used to extend the WHOI data. The left panels of Fig. 4 show the time series of the first three ASIS data EOFs. One can see that when the one-hour window reaches the internal waves (at the center time ~10:35:00Z), the EOFs begin to evolve. The data variance (measured in each window) also starts to increase (see the upper right panel). The data variance reaches its maximum when the center of the window is right at the wave front.

The lower right panel of Fig. 4 shows the fraction of the data variance each EOF captures. The fractions are time dependent, as are the EOFs, illustrating the need for the moving window processing and weighted-EOF approach. Coupling this information with the EOF shape plots, one can visualize the depth distribution of the data variance. For example, at 11:15:00Z about

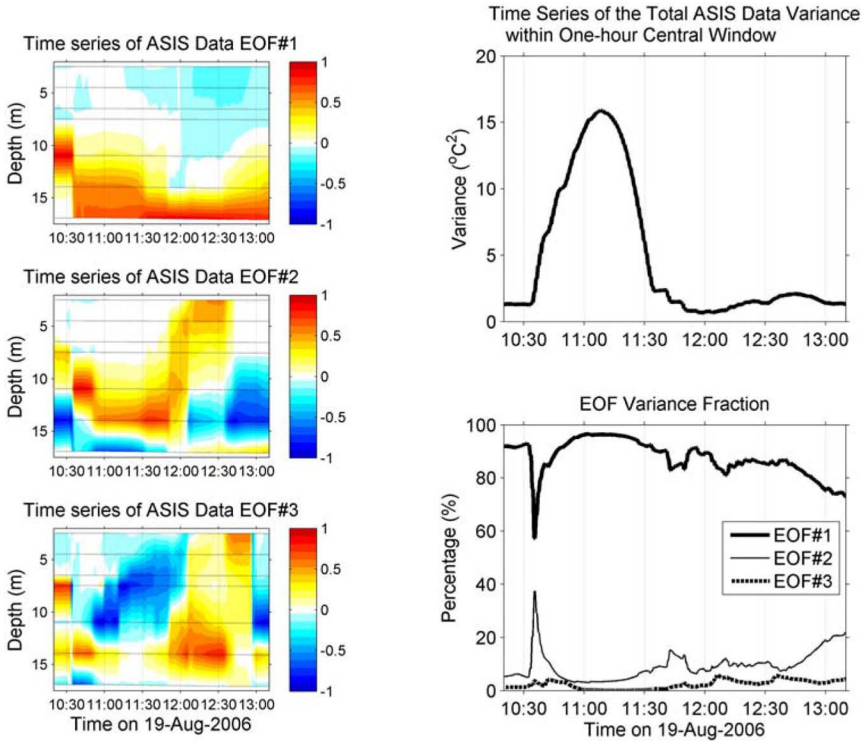

Fig. 4. ASIS data EOFs during the August 19th wave event. Right panels show the statistics derived from a one-hour central windowed data. Left panels are linear interpolation of the seven-point discrete EOFs, and the horizontal dashed lines are the sensor depths.

95% of the variance is captured by the first EOF, with the energy distributed over the depth range 10–17 m. Note that the EOF is closely associated with the data coherence structure, and the EOF shape indicates that the lower two sensor data are correlated with other sensors. Because of this correlation, it is possible to recover conditions at the top five ASIS sensor depths from the deeper measurements.

C. Merging Performance

An important question that must be answered concerns the reliability of the merging procedure. Here, three error analyses are presented.

1) August 19 Wave Example: The mixed layer structure measured by the ASIS buoy appears reasonably captured and preserved in the merged profile example of Section III-B (Fig. 3). A statistical analysis is performed here to quantify underlying errors in the result. One source of error was identified in the derivation: the process of data interpolation of primary data to secondary sensors depths. The interpolation error is defined as $\mathbf{e} = \hat{y}_{\rm pri}(\mathbf{z}_2, t) - y_{\rm pri}(\mathbf{z}_2, t)$, where the hat indicates estimated data value and the other value is the actual (unmeasured) primary data value at depth $\mathbf{z}_2$. With straightforward linear algebra, it can be seen how these errors propagate to the merged profiles.

We first obtain the errors $\mathbf{e}_\alpha$ in the EOF coefficient estimates $\hat{\boldsymbol{\alpha}}$ that are caused by the interpolation error $\mathbf{e}$. The variance of $\mathbf{e}_\alpha$ can be found using (7), $\Sigma_{\hat{\boldsymbol{\alpha}}} = \mathbf{B}\boldsymbol{\Sigma}\mathbf{B}^T$, where $\boldsymbol{\Sigma}$ is the variance of error $\mathbf{e}$, and where (7) is written as $\hat{\boldsymbol{\alpha}} = \mathbf{B}\Delta\mathbf{y}$. $\boldsymbol{\Sigma}_{\hat{\boldsymbol{\alpha}}}$ can be further propagated to the merging error. Using (4), it is found $\boldsymbol{\Sigma}_{\hat{\mathbf{y}}} = \mathbf{H}\boldsymbol{\Sigma}_{\hat{\boldsymbol{\alpha}}}\mathbf{H}^T$. Substitution yields the final equation for the merging error variance

$$\boldsymbol{\Sigma}_{\hat{\mathbf{y}}} = \mathbf{HB}\boldsymbol{\Sigma}\mathbf{B}^T\mathbf{H}^T. \tag{12}$$

The lowest panel of Fig. 3 shows the detailed time-dependent merging error variances (the diagonal terms of $\boldsymbol{\Sigma}_{\hat{\mathbf{y}}}$) in the August 19 wave event. The error estimates appear suitably small. Significant errors are found around time 10:30:00Z. Examining the EOF shape shown in Fig. 4 can explain this. The EOF variance fraction plot (the lower right panel of Fig. 4) shows about 90% of the variance in the first EOF, but at the time in question this EOF shape is close to zero at the overlapped depths (unlike at other times), indicating small data correlation between top five and lower two sensors. Thus, the merging method cannot be expected to work properly for 90% of data variability. However, because the method uses all EOFs with weights according to its energy spectrum, it is still able to capture the other 10% of variability.

2) Merging Errors Over the Entire Period: The expression for the variance of merging errors (12) is applied to the entire data set. The right panels of Fig. 5 show the time series of error variance at three depths. The left panel shows that the merging errors generally increase with depth. The variance time series also indicates that the error variances during the period from August 8th to August 12th have peak values greater than other periods. This is because the maximum thermocline gradient is well above the lower two ASIS sensors during that interval (see the second panel of Fig. 2); in other words, there is not much statistical information about the thermocline variability contained in the data from the lower two sensors. Analysis of EOF profiles can also indicate this. (EOF profiles consistent with similar poor performance appear at the initial time period of Fig. 4.)

Performance of the objective function fitting method of Davis [2] is also shown. As described before, Davis' method is essentially a selected-EOF approach, unlike our tapered and weighted-EOF approach. Fig. 6 shows the average profiles

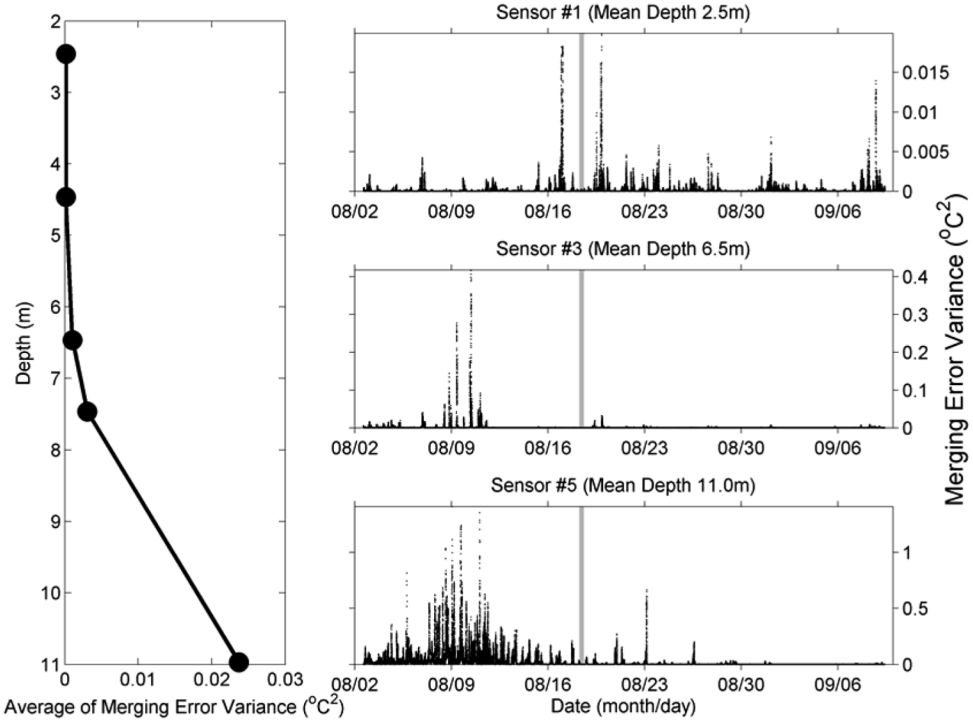

Fig. 5. Merging error due to the interpolation errors/uncertainties in the overlapped depth range. The left panel is the average variance over the entire experimental period. The right panels are variance time series at three depths, and the shaded bar indicates the time of the example shown in Figs. 3 and 4.

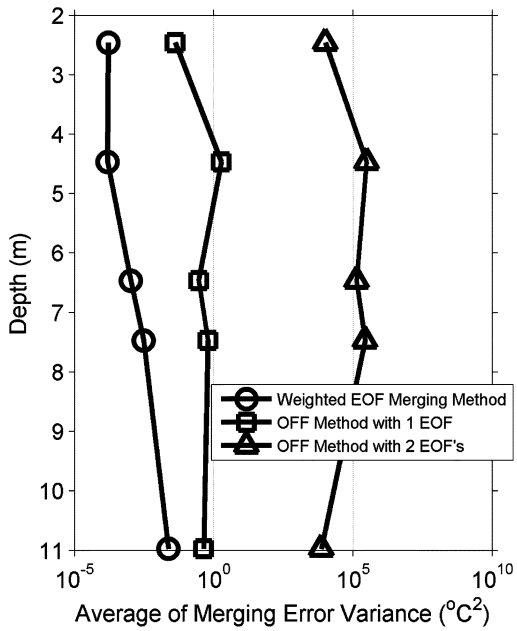

Fig. 6. Merging error comparison of the method presented in this paper (tapered and weighted EOF) and the objective function fitting (OFF) method. The x-axis (averaged variance) is in a logarithm scale.

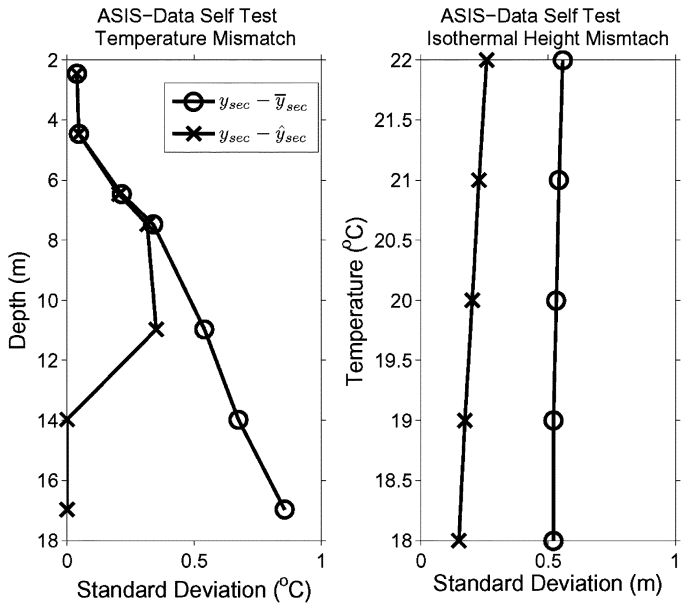

Fig. 7. ASIS-data self-test results. The standard deviation of the temperature mismatch at the sensor depths over the entire testing period from August 2nd to August 24th is shown in the left panel. The standard deviation of five selected isothermal height mismatch over the entire testing period is shown in the right panel. The lines with circles are the true perturbations calculated from original data minus moving averaged profiles (one-hour central boxcar window).

of merging error produced by our method and the method of Davis. One can see that the weighted-EOF approach performs better than the selected-EOF approach for this upper ocean data merging example.

3) ASIS Data Self-Test: The merging performance can also be tested by considering data only from the secondary location (the ASIS location in our example data set). To be more specific, the testing procedure is to compare measured secondary locations with profiles rebuilt using data from the lower two secondary sensor locations. This is consistent with using $y_{\rm sec}$ in place of $y_{\rm pri}$ in (4), continuing the process to find the EOF coefficients α_k. These then yield a result $\hat{y}_{\rm sec}$, which can then be compared against the original $y_{\rm sec}$ for accuracy.

Fig. 7 shows on the left the standard deviations of the mismatch time series $y_{\rm sec} - \hat{y}_{\rm sec}$ and, for comparison, the larger

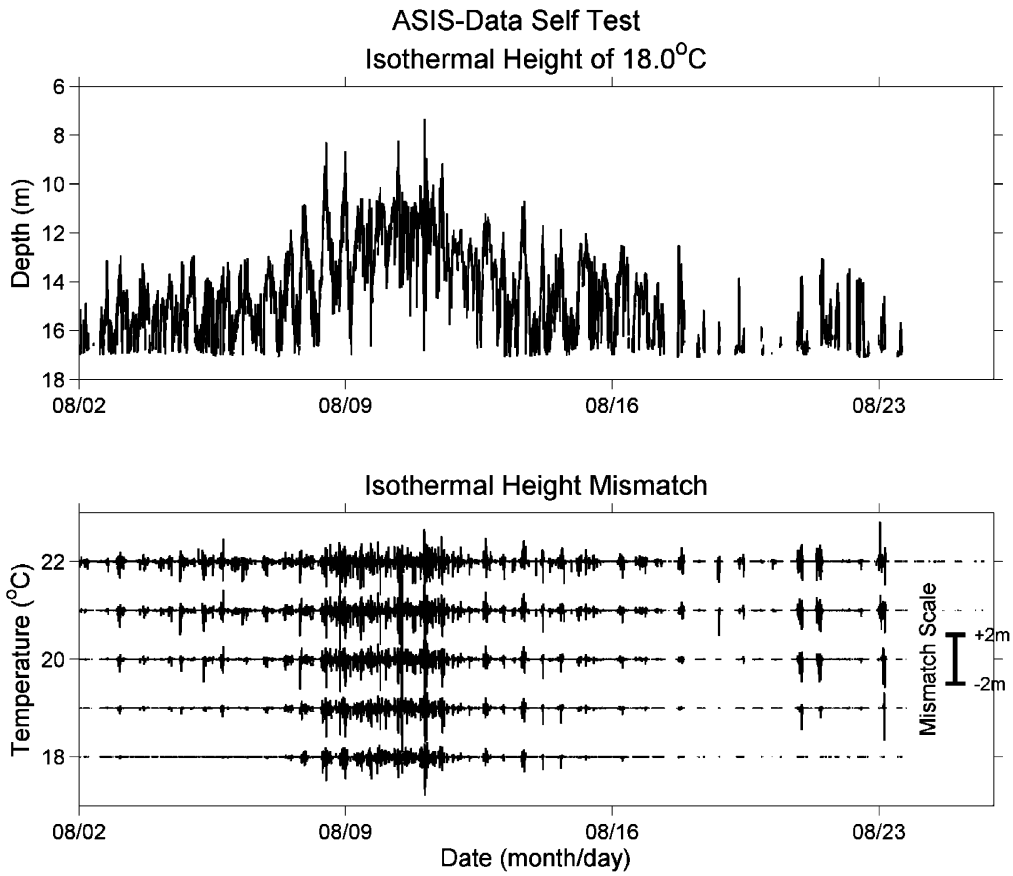

Fig. 8. Isothermal height of 18 °C of ASIS data (upper panel). Isothermal level mismatch in the ASIS-data self-test example (lower panel).

variances of the demeaned original time series. It also shows on the right the standard deviations of isothermal heights estimated from $y_{\rm sec}$, and the standard deviations of the differences between these heights and those estimated after the fitting procedure. The test shows that the profiles can be rebuilt reasonably accurately using only data from two lower end sensors, at least for this data set. Fig. 8 shows the entire time series of isothermal height mismatch, and shows in another panel the 18°C height time series which serves as a proxy for the depth of maximum thermocline gradient. The mismatch magnitudes are highest during the period from August 8th to August 12th, when the maximum gradient zone is well above the lower two sensors.

Finally, note that it is difficult to validate the assumption that temperature fluctuations at the overlapping depths of the two positions (WHOI VLA and ASIS in the SW06 example) are simply spatial and time lagged versions of the same process, as they would be for progressive waves with isotherm displacement $\eta(x - ct)$ moving a speed c through a uniform water column [i.e., $T(z)$ uniform over x]. This assumption of stationarity becomes more reliable as the distance between the two positions approaches zero.

IV. Using SW06 Merged Temperature for Sound-Speed Profile Reconstruction

This section describes salinity (S) data sources used to convert the temperature (T) profiles obtained in Section III to sound-speed profiles using Chen and Millero's formulation [15]. The results are then shown.

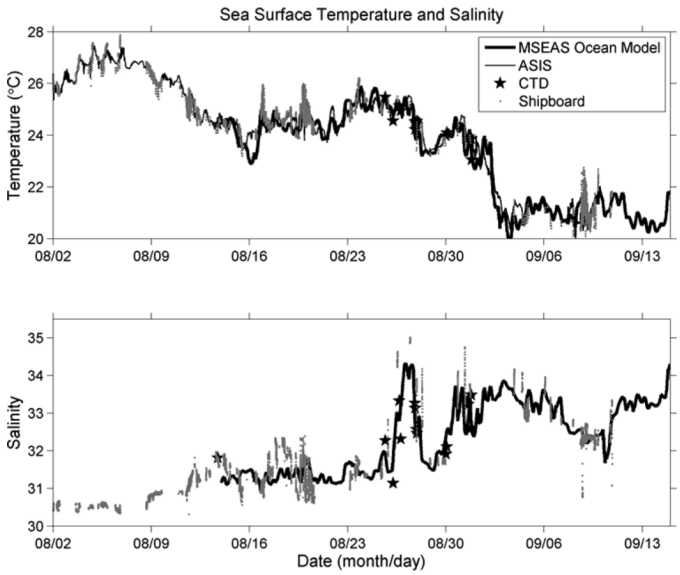

Fig. 9. Multiple sea surface data for the upper 5-m water column around the WHOI VLA (5-km radius).

A. Incorporating Salinity Information and Data-Assimilated Ocean Model Simulations

The computation of sound speed requires T, S, and pressure. Because no salinity sensors were attached to the WHOI VLA or

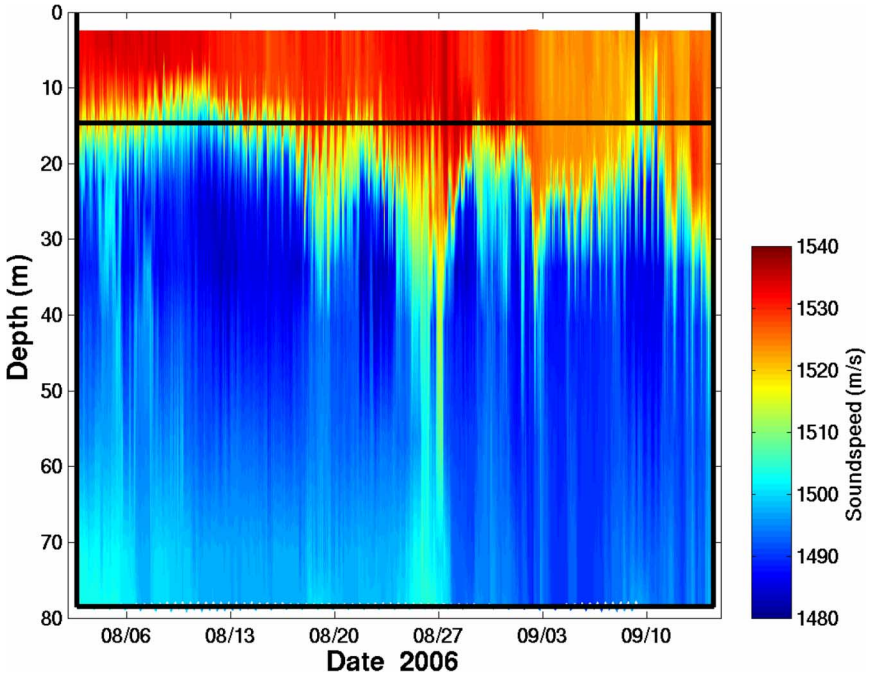

Fig. 10. Full water-column sound-speed profiles resulting from merging multiple data sources at the WHOI VLA. Boxes identify areas of different temperature data sources. The upper left box indicates the ASIS buoy data, the upper right one is the MSEAS ocean model results, and the lower big box is the WHOI VLA data. The ENV#30 data are also used for incorporating salinity, along with some assistance from MSEAS ocean model results.

ASIS buoy, salinity is estimated using data from nearby sensor suite. Environment mooring ENV#30 carried ten conductivity, temperature, and pressure sensors, yielding S and the TS relationships used to estimate S from T. This mooring was located 1530 m northwest of the WHOI VLA (Fig. 1). Measurements were taken every 30 s at the following depths: 14, 16, 20, 25, 32, 39, 47, 56, 65, and 74 m. Images of the temperature and salinity data at this site can be found in Fig. 2. The sensors, manufactured by Sea-Bird Electronics (Bellevue, WA), compute S internally from temperature, conductivity, and pressure.

The TS relationships (S as a function of T) found from ENV#30 data are employed to calculate $S(z,t)$ from $T(z,t)$ for all sensors at the VLA location. This assumes similar water masses at the two sites. This assumption is justified by the short intermooring distance (Fig. 1) and by the similarity of temperature fluctuations at the two sites (Fig. 2). A sequence of TS curves at the ENV#30 mooring (all depths included) is calculated with a moving time window (one hour in length, as in the T merging process).

Because there are no salinity data in the upper water column on mooring ENV#30 (see Fig. 2), conductivity–temperature–depth (CTD) cast data and shipboard sea surface monitoring records within 5-km radius around the WHOI VLA are used for generating TS curves to calculate $S(z,t)$ from the merged $T(z,t)$. See Fig. 9 for the available sea surface measurements.

For a short time period after the removal of ENV#30 mooring, but before SW06 was complete, TS relationships from regional model simulations were used. These were from SW06 forecasts and/or hindcasts made with the oceanographic modeling and assimilation schemes of the Massachusetts Institute of Technology (MIT, Cambridge) Multidisciplinary Simulation, Estimation, and Assimilation System (MSEAS) [16]. This system included oceanographic primitive-equation models [17] and tidal models [18] with data assimilation and uncertainty prediction [8], [19]. The primitive-equation model used here was a new free-surface version of the Harvard Ocean Prediction System (HOPS) [20] completed at MIT. The model featured a 3-km spatial resolution and saved TS fields at one-hour intervals, but could not resolve the nonlinear internal-wave field. The T and S model fields at the WHOI array location are shown in the bottom panels of Fig. 2. Note that these model simulations did not assimilate any of the SW06 mooring data utilized in this work. Note also that when no ship was near the VLA before the removal of ENV#30, MSEAS salinity information was also used for the depths where ship CTD data were ordinarily used.

In the last few days of the WHOI VLA operation, after recovery of the other moorings (no more ASIS buoy data available), the upper portion of the water column was thoroughly mixed by a large tropical storm named Ernesto that passed over the SW06 site on September 2nd. Since the nonlinear internal waves during this time were still active, our data merging strategy is to use the MSEAS ocean model and is threefold: 1) since the upper portion of the water column was well mixed, when the top of the thermocline was below the top VLA sensor ($\sim$13 m), directly extrapolate the VLA temperature data to the surface, 2) if the top of the thermocline was above the top VLA sensor, extend to the surface using the MSEAS ocean model averaged sea surface temperature, and 3) directly use the predicted salinity from the MSEAS ocean model because there were no conductivity measurements during this time.

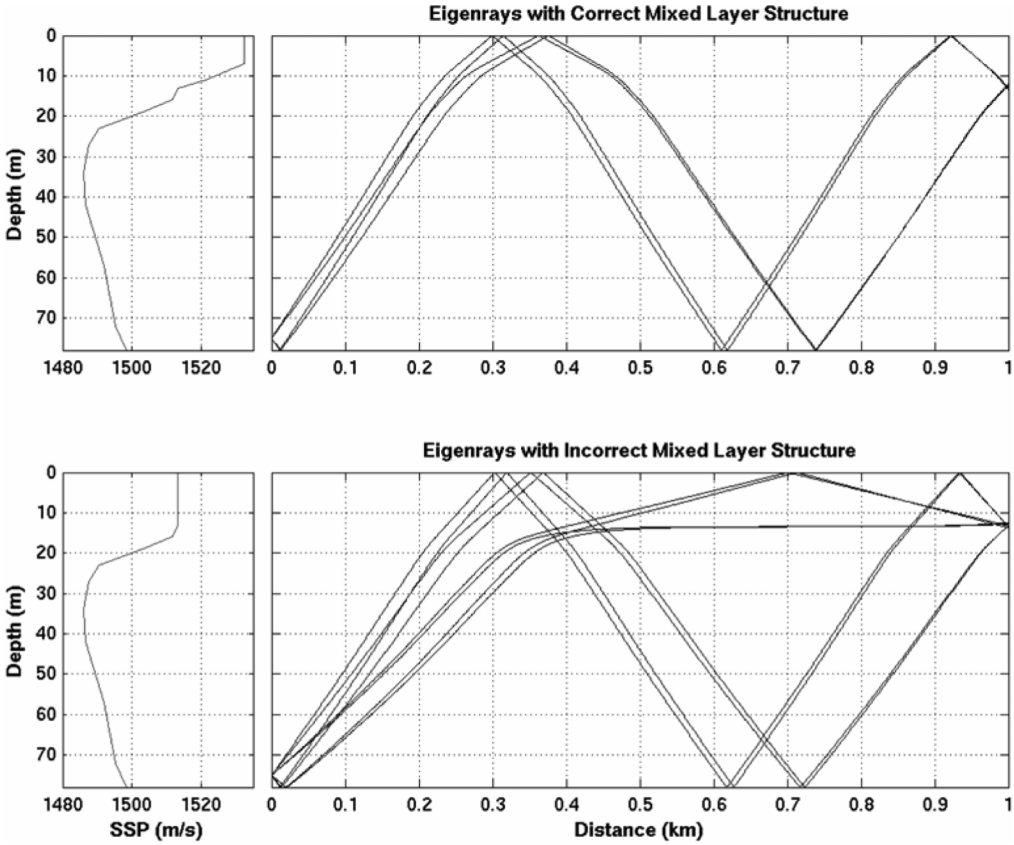

Fig. 11. Ray tracing comparison of the merged sound-speed profile (upper) and an extrapolated sound-speed profile (lower). The sound-speed profile at 12:00:00Z on August 10th is used. The merged profile has correct mixed layer structure, but the extrapolated does not. As a result, four incorrect eigenrays are found in using the incorrect extrapolated profile. The arrival time of each eigenray is summarized in Table II.

B. Final Sound-Speed Profiles and Improvements of Ray Tracing Modeling

Sound-speed profiles were computed for the entire duration of SW06 using the merged temperature profiles and the salinity estimates described above. The final full water-column sound-speed estimates are shown in Fig. 10. The overall performance of this data merging approach on capturing the mixed layer structure is good, and capturing mixed layer structure is essential for many acoustic modeling applications. An acoustic ray tracing modeling example shown next illustrates that neglecting detailed mixed layer structure will produce incorrect ray paths.

Accuracy in numerical modeling of sound passing through the upper water column can be ensured with a better mixed layer structure estimate. This is important for applications such as long-baseline navigation or grazing-angle-dependent surface and seafloor reflection or reverberation studies. Comparison of ray paths generated using a merged profile and a linearly extrapolated VLA profile which does not have correct mixed layer structure illustrates this point (Fig. 11). A sound-speed profile for a time period with no internal waves (12:00:00Z on August 10th) is chosen for this example. To mimic signals of the VLA long-baseline array navigation system, a source mounted on the bottom (acoustic interrogator) is placed 1 km away from a receiver 13 m below the sea surface. With the extrapolated mixed layer structure, four incorrect eigenrays are found (bottom panel of Fig. 11). The arrival time of each eigenray in both models is summarized in Table II, and the same type of ray path is grouped for comparison. An error in sensor position on the order of 20 m will occur if one uses a simple extrapolated profile and incorrect eigenrays for long-baseline navigation.

V. Discussion

The most significant advantages of the EOF merging technique are that the mixed layer structures measured by the ASIS buoy are well preserved in the merged profiles, and that the arrival time differences of nonlinear internal waves at the WHOI VLA and the ASIS buoy can be systematically and automatically accounted for. The EOF technique is simpler than sliding the ASIS data time series to match with the VLA data, which would require determining the propagating speeds and directions of the hundreds of internal waves seen in the data. In addition, such sliding of the secondary data set could lead to discontinuities (field or derivatives), which would affect numerical modeling of sound propagation. If a filter was then utilized to smooth out these discontinuities, the more rapidly varying fields (e.g., the internal waves) could be smoothed out.

The length of the moving time window used in the temperature data merging process was decided empirically to be one hour using iteration and examination of EOFs and merged profiles, particularly during nonlinear internal wave events. It was found that the window should cover at least a few cycles of internal wave motion so that sufficient statistic information can be obtained. If the window is too short, the scheme does not properly track the motion of internal waves as they propagate from one mooring to another. On the other hand, if the window

TABLE II
ACOUSTIC RAY TRACING ARRIVAL TIMES FOR DIFFERENT EIGENRAYS USING A MERGED SOUND-SPEED PROFILE AND AN EXTRAPOLATED SOUND-SPEED PROFILE. THE EXACT RAY PATHS CAN BE SEEN IN FIG. 11. THE RAY PATH LABELS ARE DESIGNATED AS THE FOLLOWING: B INDICATES A BOTTOM REFLECTION, S INDICATES A SURFACE REFRACTION, AND R INDICATES REFRACTION IN THE WATER COLUMN

Ray path label	Arrival times using the merged soundspeed profile with correct mixed layer (seconds)	Arrival times using the extrapolated soundspeed profile with incorrect mixed layer (seconds)
R		0.6675
BR		0.6679
RS		0.6681
BRS		0.6686
SB	0.6830	0.6845
BSB	0.6839	0.6853
SBS	0.6856	0.6875
BSBS	0.6864	0.6884

is too long, the EOFs can be less than optimal for this procedure and the merged profiles are observed to miss the detailed water-column variability. Rigorous theoretical analysis of the window length requires further investigation, but we think that the internal wave statistics in the one-hour window length are well correlated with the moorings used here.

In the data merging process reported here, the effect of buoy tilt on the ASIS sensor depths is considered, but the motion of the VLA and ENV#30 moorings is neglected because it is found to be generally small [14]. However, the derived sound-speed profiles might still have potential errors due to lack of exact sensor depths on the VLA and ENV#30 moorings. This work has carefully corrected the tidal effects on the nominal sensor depths, but it did not correct for the exact mooring motion. Long-baseline navigation on the VLA may provide us a guideline to judge the uncertainties of the final estimates. In general, during periods when the array motion was greater than average (in 25% of the time the tilt angle is greater than 1.5°, but in less than 5% of the time it is greater than 2.5°), the merged data should be used with care. One should also notice that the long-baseline navigation technique is coupled with sound-speed estimates. Thus, it would be more proper to do simultaneous array navigation and sound-speed estimation. However, this is beyond the scope of this paper, and it is left for the future.

VI. CONCLUSION

Time-varying EOF-based methods to merge time-varying data profiles from multiple sources into profiles indicative of conditions at a single site have been presented. An application was presented and studied, using temperature data from two SW06 moorings, a few hundred meters apart. Full water-column sound-speed profile estimates during SW06 were obtained from these reconstructed temperature profiles and salinity measurement from either nearby mooring data or the MIT-MSEAS ocean model simulations. Such profiles can be used for accurate acoustic modeling. The data merging quality was examined for accuracy over a broad time scale, from minutes to days.

The method explained here has general practicality, and its advantages are summarized. It has been shown that the water layer structure measured by one partial depth system can be accurately preserved in the merged profiles at another location in a spatially stationary region. The arrival time differences of internal waves at the two locations can be systematically and automatically adjusted without knowing exact internal wave propagation speeds and directions. The merged profiles provide a more complete oceanographic view of the local water-column variability at the chosen location. The profiles have been used in other acoustics propagation modeling endeavors and have improved acoustic real data and model comparisons [21], [22].

ACKNOWLEDGMENT

The authors would like to thank H. Graber and N. Williams for providing them with the ASIS mooring data. They would also like to thank the WHOI deployment/recovery team, along with the captains and crews of the *R/V Knorr, R/V Oceanus*, and *R/V Endeavor*. The authors would also like to thank SW06 Principal Investigator J. F. Lynch for his guidance and encouragement on this paper. P. F. J. Lermusiaux and P. J. Haley would like to thank W. G. Leslie and O. G. Logutov for their real-time contributions. The authors would also like to thank the reviewers for carefully reviewing this manuscript and for providing several key suggestions.

REFERENCES

[1] W. J. Emery and R. E. Thomson, *Data Analysis Methods in Physical Oceanography*, 2nd rev. ed. Amsterdam, The Netherlands: Elsevier, 2001, ch. 4.

[2] R. E. Davis, "Objective mapping by least squares fitting," *J. Geophys. Res.*, vol. 90, no. C3, pp. 4773–4777, 1985.

[3] L. R. LeBlanc and F. H. Middleton, "An underwater acoustic sound velocity data model," *J. Acoust. Soc. Amer.*, vol. 67, pp. 2055–2062, 1980.

[4] A. E. Newhall, J. F. Lynch, C. S. Chiu, and J. R. Daugherty, "Improvements in three-dimensional raytracing codes for underwater acoustics," in *Computational Acoustics: Ocean-Acoustic Models and Supercomputing*, D. Lee, Cakmak, and Vichnevetsky, Eds. Amsterdam, The Netherlands: North-Holland, 1990, pp. 169–185.

[5] T. F. Duda and C. R. Rehmann, "Systematic microstructure variability in double-diffusively stable coastal waters of nonuniform density gradient," *J. Geophys. Res.*, vol. 107, pp. 3145–3145, 2002.

[6] P. F. J. Lermusiaux, "Data assimilation via error subspace statistical estimation. Part II: Middle Atlantic Bight shelfbreak front simulations and ESSE validation," *Monthly Weather Rev.*, vol. 127, no. 7, pp. 1408–1432, 1999.

[7] F. P. Bretherton, R. E. Davis, and C. B. Fandry, "A technique for objective analysis and design of oceanographic experiments applied to MODE-73," *Deep-Sea Res.*, vol. 23, pp. 559–582, 1976.
[8] P. F. J. Lermusiaux, "Adaptive modeling, adaptive data assimilation and adaptive sampling," *Physica D*, vol. 230, pp. 172–196, 2007.
[9] T. P. Sapsis and P. F. J. Lermusiaux, "Dynamically orthogonal field equations for continuous stochastic dynamical systems," *Physica D*, vol. 238, pp. 2347–2360, 2009, DOI: 10.1016/j.physd.2009.09.017.
[10] P. F. J. Lermusiaux, P. Malanotte-Rizzoli, D. Stammer, J. Carton, J. Cummings, and A. M. Moore, "Progress and prospects of U.S. data assimilation in ocean research," *Oceanography*, vol. 19, Special Issue on "Advances in computational oceanography", no. 1, pp. 172–183, 2006.
[11] D. J. Tang, J. N. Moum, J. F. Lynch, P. Abbot, R. Chapman, P. H. Dahl, T. F. Duda, G. Gawarkiewicz, S. Glenn, J. A. Goff, H. Graber, J. Kemp, A. Maffei, J. D. Nash, and A. Newhall, "Shallow Water'06, a joint acoustic propagation/nonlinear internal wave physics experiment," *Oceanography*, vol. 20, pp. 156–167, 2007.
[12] C. Wunsch, *The Ocean Circulation Inverse Problem*. Cambridge, U.K.: Cambridge Univ. Press, 1996, ch. 3.
[13] H. C. Graber, E. A. Terray, M. A. Donelan, W. M. Drennan, J. C. van Leer, and D. B. Peters, "ASIS—A new air-sea interaction spar buoy: Design and performance at sea," *J. Atmos. Ocean. Technol.*, vol. 17, no. 5, pp. 708–720, 2000.
[14] A. Shmelev, *Private communication.* Apr. 2008.
[15] C. T. Chen and F. J. Millero, "Speed of sound in seawater at high pressures," *J. Acoust. Soc. Amer.*, vol. 62, pp. 1129–1135, 1977.
[16] MSEAS Group, "The multidisciplinary simulation, estimation, and assimilation systems," Dept. Mech. Eng., Massachusetts Inst. Technol., Cambridge, MA, Reports in Ocean Science Engineering, 2010 [Online]. Available: http://mseas.mit.edu/, http://mseas.mit.edu/codes
[17] P. J. Haley, P. F. J. Lermusiaux, W. G. Leslie, and A. R. Robinson, "Harvard Ocean Prediction System (HOPS)," 2006 [Online]. Available: http://mseas.mit.edu/HOPS
[18] O. G. Logutov and P. F. J. Lermusiaux, "Inverse barotropic tidal estimation for regional ocean application," *Ocean Model.*, vol. 25, pp. 17–34, 2008.
[19] P. F. J. Lermusiaux, "Uncertainty estimation and prediction for interdisciplinary ocean dynamics," *J. Comput. Phys.*, vol. 217, Special Issue of on "Uncertainty quantification", pp. 176–199, 2006, J. Glimm and G. Karniadakis, Eds.
[20] P. J. Haley Jr. and P. F. J. Lermusiaux, "Multiscale two-way embedding schemes for free-surface primitive-equations in the multidisciplinary simulation, estimation and assimilation system (MSEAS)," *Ocean Dyn.*, 2010, sub-judice.
[21] M. S. Ballard, K. M. Becker, and J. A. Goff, "Geoacoustic inversion for the New Jersey shelf: 3-D sediment model," *IEEE J. Ocean. Eng.*, vol. 35, no. 1, pp. 28–42, Jan. 2010.
[22] J. Yang, D. Rouseff, D. J. Tang, and F. S. Henyey, "Effect of the internal tide on acoustic transmission loss at midfrequencies," *IEEE J. Ocean. Eng.*, vol. 35, no. 1, pp. 1–11, Jan. 2010.

Ying-Tsong Lin (M'10) received the B.S. degree in hydraulic and ocean engineering from National Cheng Kung University, Tainan, Taiwan, in 1996 and the M.S. degree in naval architecture and ocean engineering and the Ph.D. degree in engineering science and ocean engineering from National Taiwan University (NTU), Taipei, Taiwan, in 1998 and 2004, respectively.

From 2002 to 2003, he was a Guest Investigator at the Applied Ocean Physics & Engineering (AOP&E) Department, Woods Hole Oceanographic Institution (WHOI), Woods Hole, MA. After receiving his Ph.D. degree, he began a half-year postdoctoral appointment at Underwater Acoustics Laboratory, NTU, after which he worked at WHOI as a Postdoctoral Researcher. He currently holds the position of an Assistant Scientist at the AOP&E Department, WHOI. His research interests include shallow-water acoustic propagation, acoustical oceanography, geoacoustic inversion, and underwater sound source localization.

Dr. Lin is a member of the IEEE Oceanic Engineering Society and the Acoustical Society of America.

Arthur E. Newhall (M'07) received the B.S. degree in mathematics from the University of Maine at Orono, Orono, in 1985.

He is a Research Specialist at the Applied Ocean Physics & Engineering (AOP&E) Department, Woods Hole Oceanographic Institution (WHOI), Woods Hole, MA. His current interests include ocean acoustic propagation modeling, acoustical oceanography, software engineering, and music.

Mr. Newhall is a member of the Acoustical Society of America.

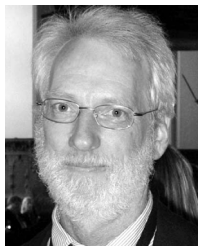

Timothy F. Duda (M'05–SM'09) received the B.A. degree in physics from Pomona College, Claremont, CA, in 1979 and the Ph.D. degree in oceanography from the Scripps Institution of Oceanography, University of California, San Diego, in 1986.

He worked at the University of California, Santa Cruz, from 1986 to 1991. He has been a Scientist at the Woods Hole Oceanographic Institution, Woods Hole, MA, since 1991. His three primary fields of study are ocean acoustic propagation, ocean internal gravity waves, and ocean mixing processes. His research has included physical process studies, development of new measurement tools, and computational acoustic modeling.

Dr. Duda is a member of the IEEE Oceanic Engineering Society. He is also a member of the American Meteorological Society, the American Geophysical Union, and the Acoustical Society of America.

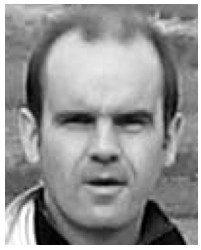

Pierre F. J. Lermusiaux (M'09) received B&M degrees in mechanical engineering (highest honors and Jury's congratulations) from Liege University, Liege, Belgium, in 1992 and the S.M. and Ph.D. degrees in engineering sciences from Harvard University, Cambridge, MA, in 1993 and 1997, respectively.

Currently, he is an Associate Professor of Mechanical Engineering, Massachusetts Institute of Technology (MIT), Cambridge. His current research interests include physical and interdisciplinary ocean dynamics, from submesoscales to interannual scales. They involve physical–biogeochemical–acoustical ocean modeling, optimal estimation and data assimilation, uncertainty and error modeling, and the optimization of observing systems.

Dr. Lermusiaux has held Fulbright Foundation Fellowships, was awarded the Wallace Prize at Harvard in 1993, presented the Ogilvie Young Investigator Lecture in Ocean Engineering at MIT in 1998, was awarded a Doherty Associate Professorship in Ocean Utilization by MIT in 2009 and a Spira Distinguished Teaching award by MIT in 2010. He is a member of the Association of Engineers of Liege University, Friends of the University of Liege, the Royal Meteorological Society, the American Geophysical Union, Oceanography Society, the American Association for the Advancement of Science, and the Society for Industrial and Applied Mathematics.

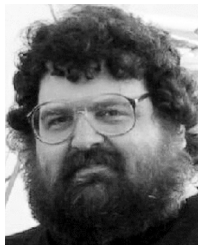

Patrick J. Haley received the B.S. degree in physics from Siena College, Loudonville, NY, in 1984 and the Ph.D. degree in applied mathematics from Northwestern University, Evanston, IL, in 1991.

From 1991 to 2006, he worked in ocean modeling and forecasting at Harvard University, Cambridge, MA, first as a Postdoctoral Researcher and then as a Research Scientist. Since 2007, he has been a Research Scientist at the Massachusetts Institute of Technology (MIT), Cambridge. His research interests include multidisciplinary ocean modeling and forecasting.